

Research Article

Bio-Photonic Sensor Using Structurally Chiral Mediums as a Basal Cancer Cell Detection

N. Ghorani*, a, A.Madania, S. Roshan Entezarb

a Department of Laser and Optical Engineering, University of Bonab, Bonab, Iran*b* Department of Physics, Tabriz University, Tabriz, Iran*Corresponding author, Email: Nadia.ghorani@ubonab.ac.ir

DOI: 10.71498/ijbbe.2024.1192716

ABSTRACT

Received: Dec. 12, 2024, Revised: Feb. 11, 2025, Accepted: Feb. 23, 2025, Available Online: Mar. 18, 2025

In this article, a high-accuracy novel optical biosensor consisting of a structurally chiral medium (SCM) with $42m$ point group symmetry and a silver metallic defect layer under the Sarid configuration as a theoretical and computational study has been investigated. We used incident light with p polarization and used the 4×4 transfer matrix method for absorption spectrum calculations. Surface plasmon polaritons (SPP) modes at the interface between a metallic layer and SCM have also been investigated. One of the advantages of using the SCM in this configuration is that it allows us to have several plasmonic and waveguide modes. We have also determined the difference between plasmonic modes and waveguide modes. This configuration creates an open assay interface for real-time detection of the interaction with extremely high sensitivity. The resonance angles observed in the absorption spectrum are very sensitive to changes in the fluid placed on top of the sensor and this sensor has a very high-quality factor that distinguishes it from other sensors. The effect of the tilt angle of the SCM has also been investigated. These combinations make the proposed designed sensor unique for performing label-free bioassays in the detection of cancer cells. The basis of this research is to detect cancer cells, which the designed sensor can detect with high sensitivity factors.

KEYWORD

Structurally chiral medium, Surface plasmon polariton, p polarized, Transfer matrix method, Plasmonic mode.

I. INTRODUCTION

In recent decades, structurally chiral materials (SCMs) have significant attention due to their unique properties and potential applications in various fields [1]. An SCM is characterized as a non-homogeneous and anisotropic material

with a relative permittivity dyadic that varies helicoidally along a predetermined direction. Examples of SCMs include chiral elastomers, cholesteric liquid crystals, and sculptured thin films, which exhibit the circular Bragg phenomenon (CBP). The CBP leads to the near-total reflection of co-handed circularly

polarized plane waves at specific spectral regimes while allowing significant transmission of cross-handed waves [2_4].

The interaction between surface plasmons and photons at the interface of a metal and a dielectric material gives rise to surface quasiparticles termed surface plasmon polaritons (SPPs) [5]. In the coupling of photons and SPPs in practical configurations like the Kretschmann and Otto setups, the phenomenon of total internal reflection is employed [6]. When the interface of a metal and a periodically non-homogeneous dielectric material is considered, the propagation and excitation of SPP waves can be enhanced. SCMs serve as effective mediums for observing surface multi-plasmonic phenomena, leading to applications in multianalyte chemical sensors [7]. SPP waves often suffer from short propagation lengths due to metal damping losses. To address this limitation, the Sarid configuration has been proposed, where a metal thin film is positioned between two dielectric materials atop a high-index prism, forming a Three-layer composite capable of achieving propagation lengths on the order of micrometers via suitable structural parameters. SPP waves can be studied through two primary methods: the canonical boundary value problem, which is fundamentally theoretical, and the prism-coupled configuration, which combines both experimental and theoretical approaches. Research indicates that results obtained from both methods align closely [8,9].

Cancer of any organ manifests itself in the changes and malfunctions in the organ's function. Basal carcinoma is a common type of skin cancer that affects parts of the skin due to a lot of exposure to sunlight. Over time, UV rays can damage the DNA of skin cells, and Basal cells play a role in the process of creating new skin cells. When the DNA of these cells is damaged, the mutation increases the rate of reproduction, and cancer cells accumulate in that area [10,11].

Optical biosensors, for example, SCMs, photonic crystals, and surface plasmon resonance (SPR) have shown considerable

versatility and application potential in recent years. SPR sensors detect changes in the refractive index of the medium above a metal surface following analyte interaction with surface-bound ligands, which in turn indicates plasmonic surface modes' behavior. Optical biosensors convert biological interactions, including those in blood samples, into measurable optical signals, providing single-step detection, repeatability, and ease of use, thus enabling rapid and precise measurements compared to traditional diagnostic methods. Among various types of biosensors such as electrical, piezoelectric, electrochemical, mechanical, magnetic, acoustic, and optical into an observable and evaluable format [12_14].

In this work, we have developed a biosensor based on a central metal defect within a dielectric structure configured as an SCM under the Sarid configuration. We analyze the optical absorption for p-polarized plane waves as a function of incident light angles in MATLAB software to extract multiple SPP peaks from the resulting absorption spectra that demonstrate a heightened sensitivity to variations in biological samples. The Absorption of linear polarized light in this context is computed using the 4×4 Transfer Matrix Method, laying the groundwork for advanced biosensing applications.

II. METHOD

The schematic description of the proposed optical biosensor is shown in Fig. 1 in which the excitation of SPPs at the interface of an SCM and a thin metallic layer has been employed under the Sarid configuration. The structure is composed of a prism with the dielectric constant of ϵ_1 , a thin layer of Silver with the thickness of t_m and dielectric constant of ϵ_m , and a layer of SCM with the thickness of t_{SCM} and dielectric constant of ϵ_{SCM} . The area above the second SCM is filled by the fluid biomaterial. It is assumed that this structure is irradiated by a light beam in the form of a plane wave with linear polarization from the prism at

an angle θ to the x-axis. In structurally chiral mediums, the tilt angle refers to the deviation or tilting of molecules from a reference axis (usually vertical or a specific optical axis in cholesteric liquid crystal such as SCM). This angle is crucial in chiral environments, as it influences the optical properties such as light polarization, optical rotation, and light scattering. The tilt angle determines how molecules are oriented within the structure, which impacts the material's chiral properties and the way it interacts with light, including phenomena like circular dichroism and birefringence. This angle plays a significant role in controlling the optical behavior of the medium.

The pitch refers to the distance over which the molecular or structural arrangement repeats itself in a helical or spiral pattern. It represents the length required for one full rotation of the molecular alignment around an axis. The pitch plays a key role in determining the optical properties of the material, such as the wavelength of light it reflects, its color, and its overall interaction with polarized light. Changes in the pitch can significantly affect the material's optical characteristics, including its ability to rotate light and the formation of specific optical textures [15_17].

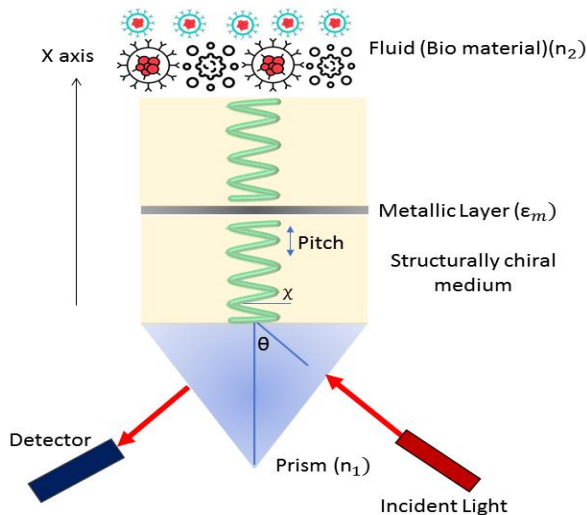


Fig. 1 The schematic description of the proposed optical biosensor.

The direction of rotation and heterogeneity of the studied structure is along the x-axis and the

electromagnetic wave enters the structure at the angle θ [18].

We have used the matrix form of Maxwell's equations in a non-magnetic environment with 4 electric and magnetic field elements $\psi(x) = (e_y(x), e_z(x), h_y(x), h_z(x))$ for the propagation of the wave [16]:

$$\frac{d\psi(x)}{dx} = ik_0 A(x) \psi_0(x) \quad (1)$$

In Eq. 1, k_0 is the wave number in the free space and $A(x)$ is 4×4 the matrix in the form of [15,18]:

$$A(x) = \begin{bmatrix} 0 & 0 & 0 & 1 \\ 0 & 0 & -1 & 0 \\ \frac{\epsilon_{zx}(x)\epsilon_{xy}(x)}{\epsilon_{xx}(x)} - \epsilon_{zy}(x) & \frac{\epsilon_{zx}(x)\epsilon_{xz}(x)}{\epsilon_{xx}(x)} - \epsilon_{zz}(x) & 0 & 0 \\ \epsilon_{yy}(x) - \frac{\epsilon_{yx}(x)\epsilon_{xy}(x)}{\epsilon_{xx}(x)} & \epsilon_{yz}(x) - \frac{\epsilon_{yx}(x)\epsilon_{xz}(x)}{\epsilon_{xx}(x)} & 0 & 0 \end{bmatrix} + \begin{bmatrix} 0 & 0 & 0 & 1 \\ 0 & 0 & -1 & 0 \\ \frac{\epsilon_{zx}(x)\epsilon_{xy}(x)}{\epsilon_{xx}(x)} & \frac{\epsilon_{zx}(x)\epsilon_{xz}(x)}{\epsilon_{xx}(x)} & 0 & 0 \\ -\frac{\epsilon_{yx}(x)\epsilon_{xy}(x)}{\epsilon_{xx}(x)} & -\frac{\epsilon_{yx}(x)\epsilon_{xz}(x)}{\epsilon_{xx}(x)} & 0 & 0 \end{bmatrix} \quad (2)$$

The dielectric tensor of an anisotropic structure in the principle coordinate system is shown in Eq. 3,

$$\epsilon = \begin{pmatrix} \epsilon_1 & 0 & 0 \\ 0 & \epsilon_1 & 0 \\ 0 & 0 & \epsilon_3 \end{pmatrix} \quad (3)$$

where the axis 3 is the distinguished axis of the SCM. To calculate the SCM dielectric tensor elements, $\epsilon_{i,j}(x)$ ($i, j = x, y, z$) in Eq. 2, we apply the tilt and rotation matrices of $T(\chi)$ and $R(x)$ to the dielectric tensor of Eq. 3 and obtain $\epsilon_{SCM}(x) = R(x)T(\chi)\epsilon T^{-1}(\chi)R^{-1}(x)$ where

$$T(\chi) = \begin{pmatrix} \cos \chi & 0 & \sin \chi \\ 0 & 1 & 0 \\ -\sin \chi & 0 & \cos \chi \end{pmatrix}, \quad (4)$$

and

$$R(x) = \begin{pmatrix} 1 & 0 & 0 \\ 0 & \cos(qx) & -\sin(qx) \\ 1 & \sin(qx) & \cos(qx) \end{pmatrix}, \quad (5)$$

with $q = \frac{2\pi}{p}$.

The rotation matrix represents a spiral motion that is performed at a constant speed and also includes the pitch of the structure and displays structural chirality [19,20].

For the propagation of the wave inside the structure, the general solution of Eq. 1 can be written as follows:

$$\psi(L) = M\psi(0) = \exp\left[ik_0 \int_0^L A(x) dx \right] \psi(0). \quad (6)$$

M is a transfer matrix in Eq. 6 that connects the wave vector ψ from the left side of the layer to the right side. We used the same method to obtain the transfer matrix of the metal layer by substituting the dielectric tensor of the chiral medium with the dielectric permittivity of the metal, ε_m . Then, we used the method presented in reference [18] to obtain the mentioned transfer matrix M for the plane-wave illumination. We also used the boundary conditions to obtain the reflection and transmission coefficients of the structure as [20]:

$$\begin{bmatrix} t_s \\ t_p \\ r_s \\ r_p \end{bmatrix} = \begin{bmatrix} t_{ss} & t_{sp} \\ t_{ps} & t_{pp} \\ r_{ss} & r_{sp} \\ r_{ps} & r_{pp} \end{bmatrix} \begin{pmatrix} a_s \\ a_p \end{pmatrix}. \quad (7)$$

The coefficients of reflections and transmissions and the amplitudes of the incident plane waves have been indicated as (r_s, r_p) , (t_s, t_p) and (a_s, a_p) , respectively in Eq. 7. To obtain the optical absorption, we use the following relationship:

$$A_{i=s,p} = 1 - \left(\sum_{j=s,p} |r_{ij}|^2 + |t_{ij}|^2 \right) \quad (8)$$

The curves obtained by plotting the optical absorption as a function of the incident angle will represent some sharp peaks which are the positions of the incident angles in which the incident photon energy is transferred to the surface plasmon polaritons.

III. RESULTS

we consider the prism-coupled method in the Sarid configuration shown schematically in Fig. 1. In the optical modeling, we consider two thin layers of SCM with the point group symmetry $\bar{4}2m$ and the dielectric constants $\varepsilon_1 = 2.7$, $\varepsilon_3 = 3.2$, the tilt angle $\chi = 45^\circ$, and length $L = 2P$ (or $L = 4P$) and the first layer of SMC is located on a prism, where $P = 595 \text{ nm}$ the pitch of the structure. A thin layer of Silver with the thickness of $t_m = 50 \text{ nm}$ and dielectric constant of the metallic layer $\varepsilon_m = -17.81 + 0.676i$ in the working wavelength (632.8 nm of He-Ne laser) is considered between the two SCM layers. First, we assume a normal and healthy biological sample named Basal cell covers the environment above the second SCM layer where the refractive index is $n = 1.360$. Also, the dielectric coefficient of the prism is $n_1 = 1.515$ in the mentioned wavelength.

The results depicted in Fig. 2 highlight the optical absorption characteristics of the structure as a function of the incident angle for two different thicknesses of the SCM layer, denoted ($L=2P$) and ($L=4P$). The Results were conducted using p-polarized light to evaluate the performance of normal Basal cells. The absorption spectra reveal several peaks that vary depending on the incident angle and in angles of 65.8° , 68.7° and 86.2° . Notably, one particular peak, marked with an arrow, shows minimal shift—almost negligible—in the excitation angle with an increase in the SCM layer thickness (L). This behavior suggests that this specific peak in 86.2° is associated with the excitation of Surface Plasmon Polaritons (SPPs), which are sensitive to the layer's

thickness but not significantly affected in this instance. In contrast, other identified absorption peaks exhibit a more pronounced shift in the excitation angle as (L) increases. These peaks are indicative of waveguide modes in angles of 65.8° and 68.7° , which respond differently to the thickness of the SCM layer compared to SPPs. Furthermore, when the optical absorption was assessed using s-polarized light, the results showed in Fig. 2 that the absorption levels in

the system were negligible across all incident angles, leading to the disappearance of the absorption peaks. This finding implies that the structure is unsuitable for biosensing applications when operating under s-polarized light conditions. As a result, this analysis establishes that a p-polarized wave is essential for effectively utilizing this structure as a biosensor, which will be the focus of the subsequent sections of the paper.

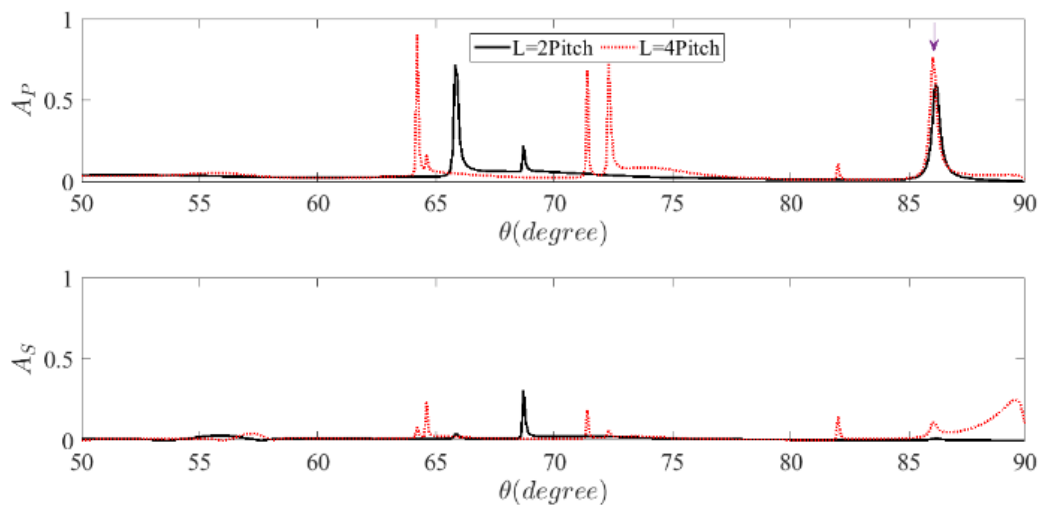


Fig. 2 The optical absorption of the structure as a function of the incident angle for two thicknesses of the SCM layer, $L = 2P$ and $L = 4P$. the results for the cases of normal Basal cells, using p-polarized waves. And the same results for the case of s-polarized waves.

To illustrate the surface plasmon polariton (SPP) modes, we have presented the electric field profiles of SPP mode within the structure, as depicted in Fig. 3. Specifically, showcase the field profiles for SPP mode at a certain incidence angle related to the case of the Basal cell. Both SPP and waveguide modes demonstrate a propagative behavior within the SCM layer, exhibiting evident localization of the electric field at the interface between the SCM and the biological sample. This phenomenon indicates a significant penetration of the evanescent wave into the sample, which is critical for sensing applications. Also, for the SPP modes, the electric field is significantly localized at the interface between the metal layer and the SCM layer. This distinct localization at different interfaces ultimately highlights the unique propagation

characteristics of SPPs and waveguide modes, emphasizing their relevance in applications such as biosensing and optical devices.

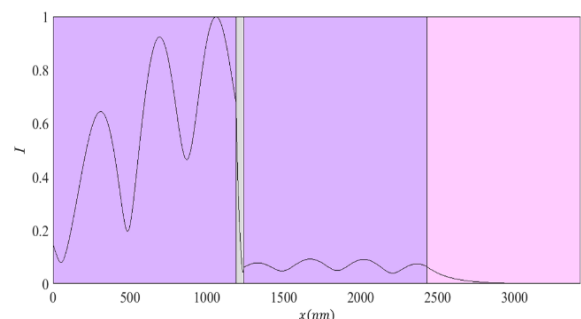


Fig. 3 The field profiles of the SPP mode correspond to the incidence angle of 86.2° .

Figure 4 shows the graph of optical absorption as a function of the incident light angle for

different thicknesses of the metal layer. According to this figure, when we consider the thickness of the metal layer to be zero, no absorption peak has been seen, and this indicates that SPPs can be excited in the vicinity of a metal and a dielectric. There is no absorption peak in the 85 nm thickness of the metal layer and it can be argued that if the thickness of the metal layer is greater than the penetration depth of the metal before the incident light reaches the interface between the metal and the SCM layer, it is absorbed or reflected and cannot transfer its energy to the SPPs and cause their excitation. On the other hand, if the thickness of the metal layer is less than its penetration depth, a greater percentage of incident light passes through the metal medium and does not have enough time to couple with surface plasmons. Therefore, thicknesses close to the penetration depth of the metal also have significant absorption. According to Figure 4, it can be seen that the peaks in the absorption spectrum are excited for the 50 nm thickness of the metal layer. It can be said that the presence of the metal layer is responsible for the formation of absorption peaks, each of which shows plasmonic or waveguide modes.

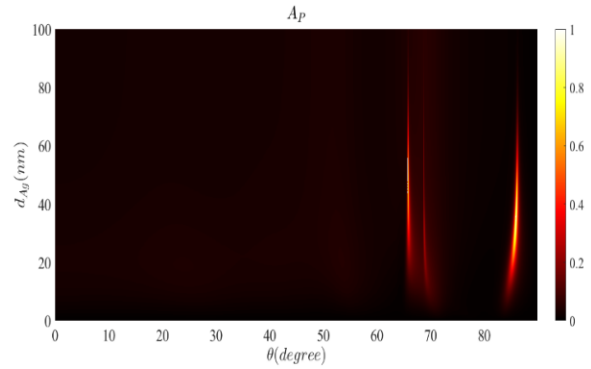


Fig.4 Optical absorption diagram for different thicknesses of the metal layer.

In this part, by examining the effect of different tilt angles of the SCM layer, we have examined the optical absorption diagram according to the angle for the designed structure. By applying different tilt angles, it can be seen that the peaks in the optical absorption graph are shifted to higher angles and the spp are excited at higher angles. The closer the tilt angle is to the vertical line, the SCM layer becomes similar to an isotropic medium, in other words, this layer has larger optical constants and the number of modes will be less. And this matter can be understood that a plasmonic and waveguide mode will appear at the junction of the metal layer and an isotropic dielectric. However, the presence of the SCM layer of specified parameters allows us to obtain several modes. The number of these modes varies by changing the specifications of the SCM and the metal layer. In summary, this proposed structure can be used as an optical sensor with the ability to create more than one mode to measure multiple analytes simultaneously in fluid matter.

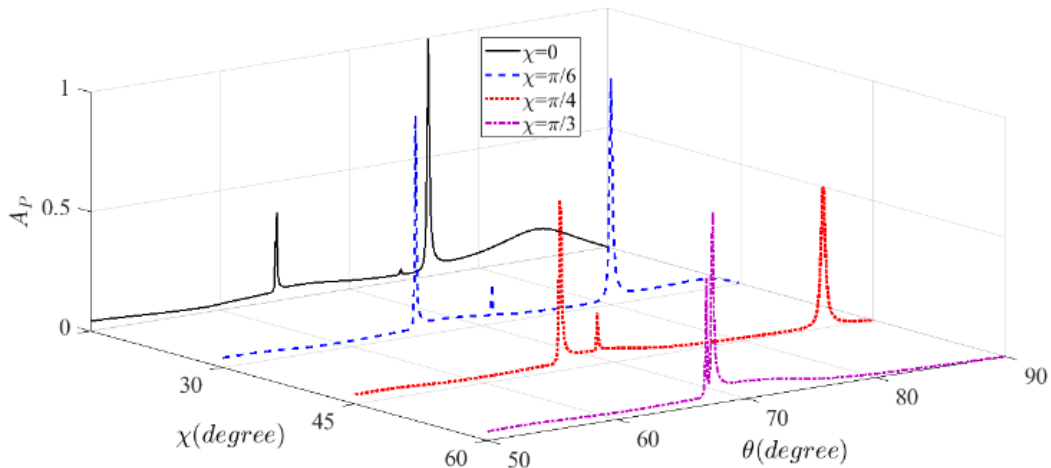


Fig.5 Optical absorption diagram for different tilt angles of SCM layer.

Fig.5 illustrates the effect of the tilt angle (χ) of the SCM layer on the optical absorption spectrum. As the tilt angle increases, the resonance peaks shift toward higher incident angles, indicating that the coupling conditions for plasmonic and waveguide modes are altered. At smaller tilt angles, the structure behaves more like an anisotropic medium, supporting multiple guided modes. However, at larger tilt angles, the system approaches an isotropic limit, leading to fewer observable resonance peaks. This effect demonstrates that adjusting the tilt angle allows for fine-tuning of the sensor's response, optimizing sensitivity for specific refractive index variations in the biological medium.

The sensitivity (S) of the designed biosensor can be expressed as the ratio of the change in resonance angle to the change in refractive index [12], for example,

$$S = \frac{\Delta\theta}{\Delta n} \quad (9)$$

The figure of merit (FOM) determines the accuracy and correctness of the data obtained from the sensor

and is calculated according to the following relationship [12]:

$$FOM = \frac{S}{FWHM} \quad (10)$$

The peak in the absorption diagram for two healthy and defective samples has been reported according to Table No. 1. This table reports the performance of the designed sensor by changing the tilt angle of the SCM layer. By examining different tilt angles, which causes changes in the light angle and, as a result, changes in the sensing parameters.

Based on Table 1, When the defective cell is replaced by the healthy cell, the changes in the refractive index bring with it changes in the absorption modes, such as the position in terms of angle, and also the reduction of the width of these modes. As the tilt angle increases, we see a gradual decrease and then an increase in FWHM. As a result, the quality factor of the sensor has a significant figure. The sensitivity of the sensor is the lowest at zero and 60° tilt angle, but with the change of the refractive index, it can detect the smallest changes of the refractive index at the tilt angles of 30° and 45° . As we expected, with the change in the refractive index of the biological material, the angle shifted, which is reported in Figure 6. One of the advantages of the presence of the SCM layer in such a sensor is that it reduces FWHM and shows the high quality of the sensor. This sensor can be used to detect the progress of diseases, which is done by comparing healthy and defective cells. By measuring the resonance angle for an unknown sample and the obtained value, it is impossible to predict the progress of

the disease, and the closer the angle changes to zero, the less progress we will have in that disease.

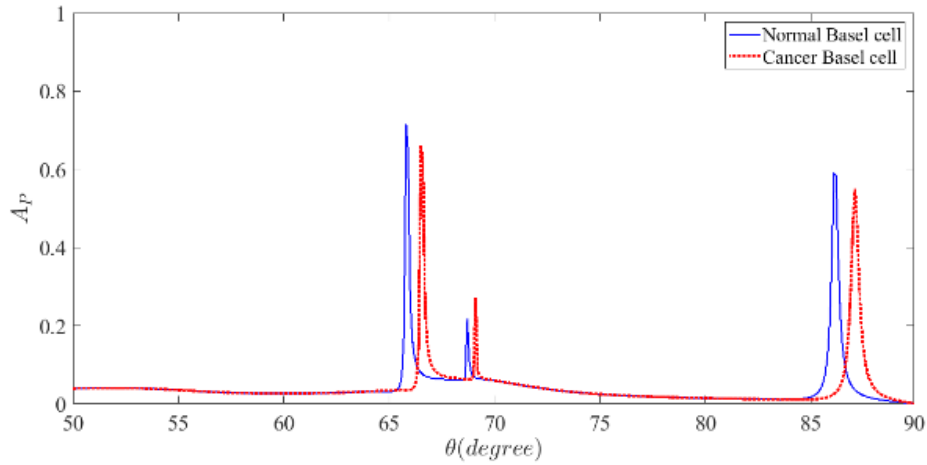


Fig.6 The absorption spectrum of the designed biosensor for healthy and cancerous samples of Basal cells.

In this section, a comparative analysis of the sensitivity and FOM of biosensors designed in recent years related to cancer is presented in Table 2. Therefore, the proposed SCM sensor can offer better performance potential due to its higher FOM compared to other sensors. By placing layers of dielectric materials, the performance of this sensor can be increased.

TABLE2. COMPARISON OF THE SCM BIOSENSOR AND PREVIOUSLY REPORTED BIOSENSORS FOR CANCER DETECTION.

Ref.	Structure	Sensitivity	FOM ($\frac{1}{RIU}$)
[21]	two-dimensional photonic crystal (PC)	15085(nm/RIU)	159.54
[22]	N-FK51A/Ag/AION/BlueP	416.85(degree/RIU)	155.94
[23]	BK7/Ag/CNT/Pt/Fe2O3	330.571(degree/RIU)	29.91
[24]	BK7/TiO2/Au/graphene	292.86(degree/RIU)	48.02
[25]	Ag/TiSi2/BP	218.6(degree/RIU)	45.26
Our Work	Prism/SCM/Al/SCM	61(degree/RIU)	575

TABLE1. SENSOR PARAMETERS FOR DIFFERENT TILT ANGLE

Cell		Sensor Parameters	$\chi = 0^\circ$	$\chi = 30^\circ$	$\chi = 45^\circ$	$\chi = 60^\circ$
Basal		$\Delta\theta$ (degree)	0.63	1.15	1.22	0.6
Normal cell	Cancer Cell	FWHM (degree)	0.2	0.1	0.2	0.15
1.36	1.38	S ($\frac{degree^\circ}{RIU}$)	31.5	57.5	61	30
		FOM ($\frac{1}{RIU}$)	157.5	575	305	200

IV. CONCLUSION

The propagation of multiple SPP waves in SCMs with a central metal defect was studied theoretically in Sarid configuration by using the transfer matrix method-based biosensor structure. The multiple SPP modes were extracted from optical absorption spectra for different structural parameters. The results showed that some branches of SPP waves had discontinuities due to their conversion to other absorption peaks such as waveguide modes or combined into other SPP modes. The key feature of this sensor is the existence of a plasmonic waveguide mode, which makes the sensor structure very sensitive to changes in the refractive index of the sensor's upper environment. The results of the optical absorption graphs as a function of the incident light angle with p polarization at the wavelength of 632.8 nm showed that more than one surface mode is emitted in the common phase.

Plasmonic modes are selected from waveguide modes by changing the thickness of the SCM layer. As the tilt angle increases, the peaks shift to higher incident light angles. The results of this work are used in biosensors and investigation of various chemical species and biomolecules that are absorbed on the surface of the SCM layer. By checking the sensor parameters for Basal cancer samples, it was checked by this sensor. The results have shown that this sensor has a high FOM quality factor with the effect of different tilt angles of the SCM environment.

REFERENCES

- [1] S. E. Swiontek, D. P. Pulsifer, and A. Lakhtakia, "Optical sensing of analytes in aqueous solutions with a multiple surface-plasmon-polariton-wave platform," *Scientific Reports*, vol. 3, no. 1, Mar. 2013.
- [2] A. Lakhtakia, M. W. McCall, J. A. Sherwin, Q. H. Wu, and I. J. Hodgkinson, "Sculptured-thin-film spectral holes for optical sensing of fluids," *Optics Communications*, vol. 194, no. 1–3, pp. 33–46, Jul. 2001.
- [3] P. D. McAtee and A. Lakhtakia, "Theory of artificial-neural-network-based simultaneous optical sensing of two analytes using sculptured thin films," *Journal of Nanophotonics*, vol. 15, no. 03, Sep. 2021.
- [4] S. Swiontek, D. Pulsifer, and A. Lakhtakia, "Optical sensing of analytes via surface multiplasmonics," *SPIE Newsroom*, Jul. 2013.
- [5] R. B. M. Schasfoort, "History and Physics of Surface Plasmon Resonance," *Handbook of Surface Plasmon Resonance*, pp. 27–59, May 2017.
- [6] S. Pal, N. Pal, Y. K. Prajapati, and J. P. Saini, "Performance Evaluation of SPR Biosensor using Metamaterial over Conventional SPR and Graphene based SPR Biosensor," *2018 5th International Conference on Signal Processing and Integrated Networks (SPIN)*, Feb. 2018.
- [7] S. Swami, F. Kayenat, and S. Wajid, "SPR biosensing: Cancer diagnosis and biomarkers quantification," *Microchemical Journal*, vol. 197, p. 109792, Feb. 2024.
- [8] F. Babaei and S. A. Seyyedi, "Excitation of Surface Plasmon-Polariton Wave at Both Interfaces of a Silver Thin Film in Two-Layer Kretschmann Geometry," *Plasmonics*, vol. 16, no. 6, pp. 2139–2146, Jun. 2021.
- [9] S. H. Hosseini-zhad and F. Babaei, "Excitation of Multiple Surface Plasmon-Polaritons by a Metal Layer Inserted in an Equichiral Sculptured Thin Film," *Plasmonics*, vol. 13, no. 6, pp. 1867–1879, Feb. 2018.
- [10] M. R. Hasan et al., "Recent development in electrochemical biosensors for cancer biomarkers detection," *Biosensors and Bioelectronics: X*, vol. 8, p. 100075, Sep. 2021.
- [11] L. Fania et al., "Basal Cell Carcinoma: From Pathophysiology to Novel Therapeutic Approaches," *Biomedicines*, vol. 8, no. 11, p. 449, Oct. 2020.
- [12] N. Ghorani, A. Madani, and S. R. Entezar, "Real-time biosensor application of structurally chiral medium for detection and sensing of plasma in human blood," *Physica Scripta*, vol. 98, no. 5, p. 055518, Apr. 2023.
- [13] F. Bayat, S. Ahmadi-Kandjani, and H. Tajalli, "Designing Real-Time Biosensors and Chemical Sensors Based on Defective 1-D Photonic Crystals," *IEEE Photonics*

- Technology Letters, vol. 28, no. 17, pp. 1843–1846, Sep. 2016.
- [14] H. Pashaei Adl, F. Bayat, N. Ghorani, S. Ahmadi-Kandjani, and H. Tajalli, “A Defective 1-D Photonic Crystal-Based Chemical Sensor in Total Internal Reflection Geometry,” *IEEE Sensors Journal*, vol. 17, no. 13, pp. 4046–4051, Jul. 2017.
- [15] M. Franco-Ortiz, A. Corella-Madueño, R. A. Rosas-Burgos, J. A. Reyes, and C. G. Avendaño, “Electrically tuned optical reflection band for an artificial helicoidal structure,” *Journal of Modern Optics*, vol. 65, no. 17, pp. 1994–2005, Jun. 2018.
- [16] C. G. Avendaño and D. Martínez, “Tunable omni-directional mirror based on one-dimensional photonic structure using twisted nematic liquid crystal: the anchoring effects,” *Applied Optics*, vol. 53, no. 21, pp. 4683, Jul. 2014.
- [17] J. A. Reyes and A. Lakhtakia, “Electrically controlled optical bandgap in a structurally chiral material,” *Optics Communications*, vol. 259, no. 1, pp. 164–173, Mar. 2006.
- [18] C. G. Avendaño, I. Molina, and J. A. Reyes, “Anchoring effects on the electrically controlled optical band gap in twisted photonic liquid crystals,” *Liquid Crystals*, vol. 40, no. 2, pp. 172–184, Oct. 2012.
- [19] I. Abdulhalim, “Analytic propagation matrix method for anisotropic magneto-optic layered media,” *Journal of Optics A: Pure and Applied Optics*, vol. 2, no. 6, pp. 557–564, Oct. 2000.
- [20] M. Faryad and A. Lakhtakia, “The circular Bragg phenomenon,” *Advances in Optics and Photonics*, vol. 6, no. 2, p. 225, Jun. 2014.
- [21] H. Miyan, R. Agrahari, S. K. Gowre, M. Mahto, and P. K. Jain, “Computational Study of a Compact and High Sensitive Photonic Crystal for Cancer Cells Detection,” *IEEE Sensors Journal*, vol. 22, no. 4, pp. 3298–3305, Feb. 2022.
- [22] S. A. Rafi et al., “Optical Based Surface Plasmon Resonance Sensor for the Detection of the Various Kind of Cancerous Cell,” *Cell Biochemistry and Biophysics*, pp.1-27, Sep. 2024.
- [23] P. Nagarajan, S. Manoharadas, V. Dhasarathan, and S. Rajeshkannan, “Cancer Detection Using Multi-layered Kretschmann Configuration-based Refractive Index Sensor,” *Plasmonics*, pp.1-12, Jun. 2024.
- [24] S. Mostufa, T. B. A. Akib, Md. M. Rana, and Md. R. Islam, “Highly Sensitive TiO₂/Au/Graphene Layer-Based Surface Plasmon Resonance Biosensor for Cancer Detection,” *Biosensors*, vol. 12, no. 8, pp. 603, Aug. 2022.
- [25] B. Karki, A. Uniyal, A. Pal, and V. Srivast, “Advances in surface plasmon resonance-based biosensor technologies for Cancer Cell detection,” *International Journal of Optics*, no. 1, pp. 1476254, Mar. 2022.